Biosensors and Bioelectronics 90 (2017) 75–82

Contents lists available at ScienceDirect

Biosensors and Bioelectronics

journal homepage: www.elsevier.com/locate/bios

Molecular visualizing and quantifying immune-associated peroxynitrite fluxes in phagocytes and mouse inflammation model

Zan Li[a], Shi-Hai Yan[a,b], Chen Chen[a], Zhi-Rong Geng[a,*], Jia-Yin Chang[a], Chun-Xia Chen[a], Bing-Huan Huang[a], Zhi-Lin. Wang[a,*]

[a] State key Laboratory of Coordination Chemistry, School of Chemistry and Chemical Engineering, Collaborative Innovation Center of Advanced Microstructures, Nanjing University, Nanjing 210093, PR China
[b] Department of Pharmacology, Jiangsu Province Hospital of TCM, Nanjing 210029, PR China

ARTICLE INFO

Keywords:
Knoevenagel condensation
$ONOO^-$
Visualizing
Quantifying
Phagocytes
Inflammation

ABSTRACT

Reactions of peroxynitrite ($ONOO^-$) with biomolecules can lead to cytotoxic and cytoprotective events. Due to the difficulty of directly and unambiguously measuring its levels, most of the beneficial effects associated with $ONOO^-$ in vivo remain controversial or poorly characterized. Recently, optical imaging has served as a powerful noninvasive approach to studying $ONOO^-$ in living systems. However, ratiometric probes for $ONOO^-$ are currently lacking. Herein, we report the design, synthesis, and biological evaluation of F_{482}, a novel fluorescence indicator that relies on $ONOO^-$-induced diene oxidation. The remarkable sensitivity, selectivity, and photostability of F_{482} enabled us to visualize basal $ONOO^-$ in immune-stimulated phagocyte cells and quantify its generation in phagosomes by high-throughput flow cytometry analysis. With the aid of in vivo $ONOO^-$ imaging in a mouse inflammation model assisted by F_{482}, we envision that F_{482} will find widespread applications in the study of the $ONOO^-$ biology associated with physiological and pathological processes in vitro and in vivo.

1. Introduction

Peroxynitrite ($ONOO^-$), a highly reactive oxygen species (hROS) (Murray et al., 2003), is a short-lived oxidant and nucleophile that is produced by the reaction of nitric oxide (•NO) and superoxide ($O_2^{\bullet -}$) radicals at diffusion-controlled rates ($\sim 1\times10^{10}\ M^{-1}\ s^{-1}$) (Gryglewski et al., 1986; Beckman et al., 1990; Radi et al., 2001). $ONOO^-$ is produced mainly in macrophages, endothelial cells, platelets, leukocytes, and neurons, and plays vital roles in physiological and pathological processes (Ahmad et al., 2009). $ONOO^-$ can directly oxidize/nitrate critical components of cells at all levels including proteins, lipids, and nucleic acids, enabling it to elicit diseases including cardiovascular and neurological disorders, cancer, and aging (Pacher et al., 2007; Szabo et al., 2007; Franco et al., 2013). However, the cytotoxic properties of $ONOO^-$ can be utilized by immune system cells to combat infecting microorganisms (Zhu et al., 1992; Denicola et al., 1993). The human immune system can utilize $ONOO^-$ to repel microbial invasion (Alvarez et al., 2011). Putative physiological roles for $ONOO^-$ include vasodilatation, inhibition of platelet aggregation, adhesion of inflammatory cells and protection against ischemia/reperfusion injury (Ronson et al., 1999; Ferdinandy, 2006; Uppu et al., 2007; Nossaman and Kadowitz, 2008).

Due to the difficulty of directly and unambiguously measuring its levels, most of the beneficial effects associated with $ONOO^-$ in vivo remain controversial or poorly characterized (Fang 2004). Thus, there is an imperative need to develop specific probes for unambiguously monitoring $ONOO^-$ levels both in vitro and in vivo (Radi, 2013).

During the past several years, researchers have designed and constructed a number of intensity-based turn-on fluorescent probes for $ONOO^-$ (Ueno et al., 2006; Yang et al., 2006; Zielonka et al., 2010; Zhang et al., 2012; Chen et al., 2013; Lin et al., 2013; Hou et al., 2014;), some of which have found utility in biological and comparative discovery studies (Peng et al., 2014; Li et al., 2015a, 2015b). Nevertheless, their use for precise $ONOO^-$ quantitation is complicated by variations in local probe concentrations, cellular microenvironments, and sample thickness. Therefore, it remains a challenge to design probes that can be robustly employed in $ONOO^-$ detection and, more importantly, in the direct analysis of its production in vitro and in vivo.

To address these issues, a BODIPY-based fluorescent scaffold was developed for the construction of F_{482} and F_{495}. This fluorophore exhibits an absorption maximum centered at 510 nm, which can be red-shifted when condensed with benzaldehyde derivatives (Lee et al., 2011; Hirata et al., 2011; Wang et al., 2011; Barba-Bon et al., 2014).

* Corresponding authors.
E-mail addresses: gengzr@nju.edu.cn (Z.-R. Geng), wangzl@nju.edu.cn (Z.-L. Wang).

http://dx.doi.org/10.1016/j.bios.2016.11.036
Received 5 September 2016; Received in revised form 10 November 2016; Accepted 14 November 2016
Available online 15 November 2016
0956-5663/

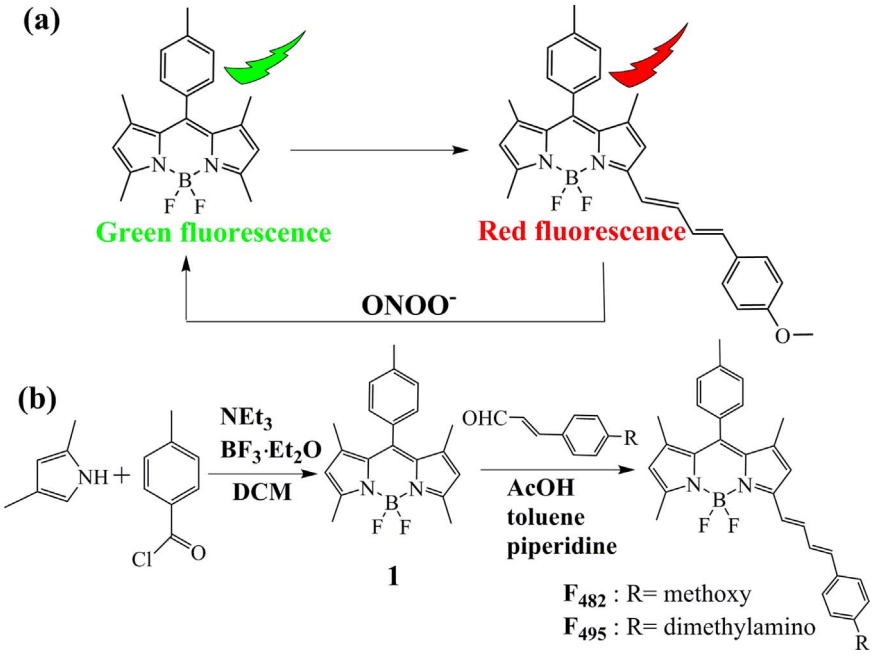

Scheme 1. (a) Design strategy for the BODIPY-based $ONOO^-$ fluorescent probes. (b) Synthesis of F_{482}, F_{495}.(For interpretation of the references to color in this figure, the reader is referred to the web version of this article.).

Such red-shifted fluorophores are desirable because of their low autofluorescence, minimal phototoxicity, and negligible interference from biomolecules when employed in live cell imaging. F_{482} and F_{495} bear a diene interconnection that acts as the recognition group. Synthesis was facile, involving a Knoevenagel condensation reaction of BODIPY with two trans-cinnamaldehyde molecules (Scheme 1b). F_{482} and F_{495} were expected to be oxidized by $ONOO^-$ to their corresponding BODIPY skeletons, which could switch on green fluorescence by cutting off the diene interconnection. To optimize the detection sensitivity, our design involves methoxyl and dimethylamino groups to be installed in the target molecules. The quantum efficiency (Φ) of F_{482} is 0.323 (606 nm), while installation of a dimethylamino group, as that in F_{495}, red-shifted the emission peak to 660 nm with a reduced Φ of 0.012.

2. Materials and methods

2.1. Materials and apparatus

All of the solvents used were of analytical grade without further purification. F_{482} (1 mM) and F_{495} (1 mM) were prepared in dimethylsulfoxide (DMSO) and stored in refrigerator for use. Stock solutions or generation of ROS/RNS were prepared according to previous report (Li et al., 2015a, 2015b). Lipopolysaccharides (LPS), phorbol 12-myristate 13-acetate (PMA), aminoguanidine (AG), apocynin were purchased from Sigma-Aldrich (USA). NMR spectra were measured on a Bruker DRX-500 spectrometer at 25 ± 1 °C with TMS as the internal standard. Mass spectrometry data were obtained on GC-TOF mass spectrometer. Fluorescence spectra were determined on a PerkinElmer LS55 fluorescence spectrometer. Absorption spectra were determined on a UV-3600 Shimadzu spectrometer. Fluorescence images were collected with Olympus Fluoview FV1000 confocal microscopy. A Lauda E100 circulating water pump was used to maintain a constant temperature at 37 °C. Ultrapure water was prepared using a Milli-Q A10 system. All pH measurements were made with a JENCO 6230 M pH meter.

2.2. Synthesis

2.2.1. Synthesis of compound 1 (Li et al. 2015b)

2, 4-Dimethyl-1H-pyrrole (2.04 g, 30.0 mmol) and p-toluoyl chloride (2.46 g, 16.0 mmol) was dissolved in 300 ml of dichloromethane under N_2. The resulting solution was stirred at room temperature under N_2 for 2 h. Triethylamine (4.65 g, 46.0 mmol) and $BF_3{\cdot}OEt_2$ (8.0 ml) was added. The solution was then stirred for 2 h at room temperature. The green organic solution was washed with brine and dried over anhydrous Na_2SO_4. The crude product was purified on a silica gel column, eluting with petroleum ether and ethyl acetate (4:1) to obtain a brick red powder 1.51 g (41.60%). ^{1}H NMR (500 MHz, $CDCl_3$), δ: 7.30 (t, J=7.6 Hz, 2H), 7.17 (d, J=8.0 Hz, 2H), 6.00 (s, 2H), 2.58 (s, 6H), 2.46 (s, 3H), 1.42 (s, 6H). ^{13}C NMR (126 MHz, $CDCl_3$), δ: 155.2, 143.2, 142.2, 138.8, 131.9, 131.6, 129.8, 127.8, 121.1, 21.4, 14.6.

2.2.2. Synthesis of F_{482}

Compound 1 (520 mg, 1.54 mmol), and trans-p-methoxycinnamaldehyde (0.95 g, 5.86 mmol) were dissolved in a mixture of toluene (50 ml), piperidine (1.0 ml) and AcOH (0.35 ml), the mixture was stirred at 120 °C under reflux for 36 h. Any water formed during the reaction was removed by using a Dean-Stark apparatus. The mixture was diluted with dichloromethane and washed with brine. The organic layer was collected, dried over Na_2SO_4 and concentrated in vacuum. The crude product was purified by silica gel column chromatography by eluting with petroleum ether and ethyl acetate (100:1) to obtain a green powder (88.9 mg, 11.2%). ^{1}H NMR (500 MHz, $CDCl_3$), δ: 7.42 (d, J=8.6 Hz, 2H), 7.31 (d, J=7.7 Hz, 2H), 7.19 (d, J=7.9 Hz, 2H), 7.09 (d, J=11.0 Hz, 1H), 7.03 (d, J=12.3 Hz, 1H), 6.98 (d, J=10.8 Hz, 1H), 6.91 (d, J=8.6 Hz, 2H), 6.73 (d, J=15.2 Hz, 1H), 6.55 (s, 1H), 6.01 (s, 1H), 3.86 (s, 3H), 2.61 (s, 3H), 2.46 (s, 3H), 1.46 (s, 3H), 1.43 (s, 3H). ^{13}C NMR (126 MHz, $CDCl_3$), δ: 159.9, 154.7, 152.7, 142.5, 140.3, 138.8, 135.8, 132.1, 129.7, 127.4, 125.5, 121.9, 121.1, 117.7, 114.3, 55.3, 29.7, 21.4, 14.7. MALDI-TOF-MS: Calcd. F_{482}, 482.23, found: 482.23.

2.2.3. Synthesis of F_{495}

Compound 1 (270 mg, 0.80 mmol), and 4-(dimethylamino)cinnamaldehyde (457 mg, 2.61 mmol) were dissovled in a mixture of toluene (50 ml), piperidine (1.0 ml) and AcOH (0.35 ml), the mixture was stirred at 120 °C under reflux for 36 h. Any water formed during the reaction was removed by using a Dean-Stark apparatus. The mixture was diluted with dichloromethane and washed with brine. The organic

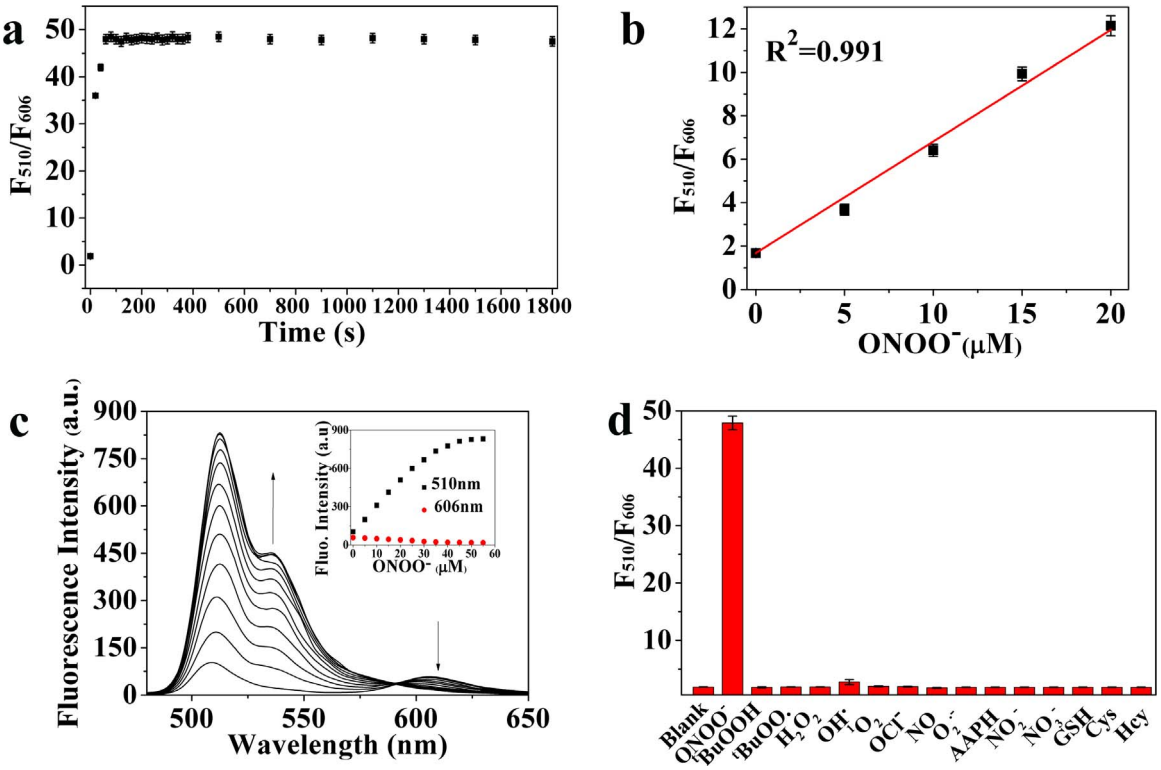

Fig. 1. Spectroscopic properties of F_{482} (5 μM) in Tris-HCl (0.02 M) solution (ethanol/Tris-HCl=1:1 v/v, pH 7.4). (a) Time course of the F_{482} fluorescence intensity ratio after the addition of 40.0 μm $ONOO^-$; (b) Ratiometric fluorescence intensity (F_{510}/F_{606}) of F_{482} as a function of $ONOO^-$ (0–20.0 μM); (c) Fluorescence response of F_{482} to increasing amounts of $ONOO^-$ (0–40.0 μM). Inset: Changes to the fluorescence intensity at 510 nm and 606 nm; (d) Ratiometric fluorescence responses (F_{510}/F_{606}) of F_{482} toward $ONOO^-$ (40.0 μM) and other ROS/RNS/RSS (100 equivalents). The excitation wavelength was 480 nm. The error bars represent ± S.D. (n=3).

layer was collected, dried over Na_2SO_4 and concentrated in vacuum. The crude product was purified by silica gel column chromatography by eluting with petroleum ether and ethyl acetate (50:1) to obtain a green powder (122.1 mg, 30.9%). ^{1}H NMR (400 MHz, $CDCl_3$), δ: 7.50 (d, J=8.8 Hz, 2H), 7.39 (d, J= 8.7 Hz, 2H), 7.28 (d, J=7.9 Hz, 2H), 7.17 (d, J=3.6 Hz, 2H), 6.68–7.07 (m, 4 H), 6.55 (d, J=23.6 Hz, 2H), 5.96 (d, J=3.8 Hz, 1H), 3.02 (d, J=5.3 Hz, 6H), 2.58 (s, 3H), 2.43 (s, 3H), 1.44 (s, 3H), 1.40 (s, 3H). ^{13}C NMR (126 MHz, $CDCl_3$), δ: 142.9, 138.6, 132.3, 129.6, 129.2, 128.2, 125.5, 120.4, 117.8,117.6, 114.5, 112.1, 111.0, 40.3, 29.7, 21.4, 14.8, 14.6. MALDI-TOF-MS: Calcd. F_{495}, 495.26, found: 495.25.

2.3. Cell imaging experiments

RAW 264.7 macrophages and human THP-1 cells were obtained from Professor Qiang Xu (NJU, Life sciences). THP-1 cells were cultured in RPMI 1640 medium with 10% heat-inactivated FBS and RAW 264.7 macrophages were cultured in DMEM medium supplemented with 10% heat-inactivated FBS. Cells were seeded in flat-bottomed plates and incubated in a humidified 5% CO_2 environment at 37 °C. F_{482} and F_{495} (5 μM) were added and cells were further incubated for 30 min, followed by washing thrice with phosphate-buffered saline (PBS). Fluorescence imaging was performed with OLYMPUS FV1000 inverted fluorescence microscope with 60× objective lens. Under the confocal fluorescence microscope, F_{482} and F_{495} were excited at 488 nm and emission was collected at 490–550 nm (green channel), excited at 543 nm and emission was collected at 570–680 nm (red channel).

2.4. Immune-stimulus

For the detection of immune associated $ONOO^-$ generation, cells were treated with LPS (1 μg/ml) for 16 h, PMA (500 nM) for 1 h and co-incubated with probes (5 μM) for 30 min. Fluorescence images were recorded at different time points: 0.5 h, 12 h, 24 h. For the $ONOO^-$-blocking experiment, cells were pre-cultured with apocynin (100 μM) for 30 min or aminoguanidine (AG) (5 mM) for 4 h, and then treated with probes (5 μM) for 30 min.

2.5. In Vivo Imaging

All animal experiments were performed in accordance with the guidelines issued by The Ethical Committee of Nanjing University. Kunming mice were given an intraperitoneal (ip) injection of LPS (200 μL, 2 mg/ml in saline) to induce acute inflammation. After 4 h, the mice were divided into three group, the first group was given an ip injection of saline (200 μL) as a control, the second group was injected ip with PMA, the third group was given an ip injection of apocynin (200 μL, 4 mM in saline). Animals were anesthetized by isoflurane and abdominal fur was removed using a razor. All the treated mice were injected ip with F_{482} (100 μL, 200 μM in saline) after 1 h. Whole body Images were acquired in 30 min by using Maestro EX in vivo imaging system. Another group were injected LPS (100 μL, 2 mg/ml in saline) on right and left rear paws. After 4 h, the left rear paw was injected 100 μL saline as a control experiment. And the right rear paw was injected100 μL PMA. After 1 h, F_{482} (100 μL, 200 μM in saline) was injected through tail vein. Images were acquired using Maestro EX in vivo imaging system in 30 min. The imaging mode is set as: green channel (Ex. 455 nm, Em. 490–540 nm) and red channel (Ex. 523 nm, Em. 560–700 nm) respectively.

3. Results and discussion

3.1. Spectroscopic properties of F_{482} and F_{495}

With F_{482} and F_{495} isolated, their spectroscopic properties were

evaluated in aqueous solution buffered to physiological pH (0.02 M Tris-HCl, ethanol/Tris-HCl=1:1 v/v, pH 7.4). Free F_{482} featured a prominent absorption band centered at 585 nm with a shoulder peak at 550 nm (Fig. S3). The corresponding emission peaks were observed at 510 nm and 606 nm with strong red fluorescence (Φ=0.323) (Fig. 1c, Fig. S5). Similarly, F_{495} exhibited 510 nm and 660 nm emission peaks but with weak red fluorescence (Φ=0.012) because of the junction with dimethylamino (Fig. S7). The fluorescence lifetime differs in terms of the various installed groups. The fluorescence lifetime of F_{482} is 3.9453 ns, whereas F_{495} has two lifetimes, 1.8161 ns (dominant, 88.8%) and 4.1559 ns (minor, 11.2%).

As the oxidation stress was predicted to oxidize the diene interconnection to form the BODIPY skeleton, the changes in the signal of red-to-green fluorescence thus furnished a ratiometric chemosensor (Drummen et al., 2004; De Cremer et al., 2010; Oushiki et al., 2010; Sun et al., 2014). Based on our strategy, the fluorescence response of F_{482} and F_{495} toward $ONOO^-$ was tested. As expected, upon addition of $ONOO^-$, the changes of F_{482} in the absorption spectra were observed, and absorption peaks at 500 nm and 530 nm appeared and became larger (Fig. S3). Interestingly, the fluorescence emission of F_{482} was enhanced by approximately 50-fold in ratiometric intensity after adding 8.0 equivalents of $ONOO^-$, along with a bright color change from red to green (Fig. 1d, Fig. S5). However, the relative emission intensity of F_{495} exhibited no significant fluorescence changes when exposed to $ONOO^-$ (Fig. S7). The time-dependent fluorescence changes (F_{510}/F_{606}) of F_{482} in the presence of $ONOO^-$ show that the reaction can be completed within 1 min and that the ratios of F_{510}/F_{606} remain constant for 30 min. Indeed, the short response time and spectrum stability were essential for the real-time detection of $ONOO^-$ (Fig. 1a). The effects of pH on F_{482} were also investigated, and the probe was found to display no corresponding fluorescence variation in the pH range of 2.0–12.0 (Fig. S4), which clearly demonstrates the stability of our probe in a physiological pH range. Furthermore, the solvent-dependency of the fluorescence signals (the ratios of F_{green}/F_{red}) was also studied in different polarity of solvents (Fig. S1, S2). The ratio value of F_{482} is constant in different solvents, which indicate that F_{482} is insensitive to the polarity of solvents. However, F_{495} is highly sensitive to the polarity of solvents, whose structure is similar to the **Compound 1** (Rurack et al., 2001). The dimethylamino group in F_{495} and **Compound 1** contribute to the solvent sensitivity while the methoxyl group makes the F_{482} insensitive to different solvents according to our obtained fluorescence data (Fig. S1, S2).

3.2. Selectivity studies for F_{482} and F_{495}

To further test the specificity of our probe towards $ONOO^-$, the fluorescence spectra of F_{482} and F_{495} were recorded before and after the addition of various ROS and RNS. Only $ONOO^-$ was observed to change the fluorescent response toward F_{482} under identical conditions (Fig. 1d , Fig. S3). The HO• radicals, rather than $ONOO^-$, caused a 20-fold relative green fluorescence enhancement for F_{495} (Fig. S10). Importantly, the other ROS/RNS and sulfhydryl-containing amino acids did not promote observable changes even when present in excess of 100 equivalents (Fig. 1d). These results suggest that F_{482} is highly selective for $ONOO^-$.

To examine the sensitivity of F_{482} to $ONOO^-$, fluorescence titration experiments were performed in Tris-HCl buffer solution. Increasing (0–8.0) equivalents of $ONOO^-$ were reacted with F_{482}, and a concentration-dependent fluorescence enhancement at 510 nm and a reduction at 606 nm were recorded after 30 min. Based on these data, a calibration curve (R^2=0.991) with a linear range of 0–20.0 μM was obtained (Fig. 1b), suggesting the potential utility of F_{482} in live cells. The detection limit of $ONOO^-$ was calculated to be 150.54 nM, which supported the potential use of our probe for ratiometrically detecting and quantifying $ONOO^-$ at low concentrations.

3.3. Proposed mechanism for sensing $ONOO^-$

Previous reports have revealed that the oxidation of a diene interconnection via either ROS/RNS results in corresponding hydroxylate or epoxide formations, and another variety of ROS results in the formation of the two main corresponding products (Drummen et al., 2004; De Cremer et al., 2010; Oushiki et al., 2010; Sun et al., 2014). The fluorescence response of F_{482} toward $ONOO^-$ is anticipated to be a consequence of the butadienyl bridge being oxidized into an extra carboxylic group in BODIPY (Scheme S1a). Oxidization of F_{495} by HO• radicals may obtain similar results (Scheme S1b). To gain experimental support for our proposal, fluorescence changes of F_{482} toward $ONOO^-$ were studied using the addition of 8.0 equivalents of $ONOO^-$ to the F_{482} solution. The emission peaks at 510 nm were enhanced, whereas those at 606 nm were reduced dramatically. This phenomenon supported our hypothesis that F_{482} was oxidized to form the BODIPY core. To shed light on the proposed assumption, the UV–visible absorption spectra were monitored following $ONOO^-$ titration. Upon the addition of $ONOO^-$, absorption peaks at 500 nm and 530 nm rose in amplitude, while those at 585 nm declined. This result indicated that the diene interconnection between the BODIPY core and the phenyl moiety of the molecule had been disrupted, as proposed in Scheme S1, and the disruption was further confirmed by LC-MS. The *m/z* signal at 367.08 represents the carboxylic functional group in the BODIPY species (calculated value is 367.14) and the *m/z* signal at 151.00 represents the carboxylic phenyl moiety (calculated value is 151.04) (Fig. S13, Scheme S1a), demonstrating the existence of a carboxylic BODIPY structure rather than the hydroxyl form reported by others. All of the results described above supported the proposed reaction with $ONOO^-$ and further confirmed the distinct fluorescence response pathway toward $ONOO^-$.

3.4. In vitro visualizing and quantifying endogenous $ONOO^-$ in stimulated phagocytes

After demonstrating the excellent responsivity and exceptional selectivity to hROS, F_{482} and F_{495} were employed for ratiometric imaging and quantifying hROS in live cells. Cell cytotoxicity tests toward RAW 264.7 cells proved that there was no significant cytotoxicity in the presence of 1–10 μM F_{482} and F_{495} for 24 h (Fig. S15). Considering the oxidative stress associated with metabolic activity in cancer and normal cells (Finkel and Holbrook, 2000), we studied whether F_{482} and F_{495} could function well in murine RAW 264.7 macrophages and human THP-1 cell lines without immune stimuli. After incubation of the phagocyte cells with either F_{482} or F_{495} (5 μM) for 30 min, the probes penetrated the cell membranes and stained the cells with clear red fluorescence from the emission channel (Fig. S16–S19). After extending the incubation times to 12 h and 24 h, the red fluorescence intensity showed negligible changes (Fig. 2), suggesting that F_{482} and F_{495} could tolerate the oxidative stress in non-immune cell lines. Owing to the exquisite fluorescence stabilities of F_{482} and F_{495}, we were motivated to perform an immunostimulation experiment in live cells. For this experiment, RAW 264.7 macrophages were immune-stimulated and then stained with 5 μM F_{482} or F_{495} for 30 min, followed by the immediate acquisition of confocal fluorescence images. As illustrated in Fig. 3a1, a2, and Fig. S20, the red fluorescence of F_{482} significantly decreased, and the green fluorescence dramatically increased, indicating that the immune-associated stimulation could be visualized by our probe. However, the red fluorescence intensity of F_{495} hardly changed (Fig. S21) probably due to the insensitivity toward immune-associated stimulation though possessing the low HO• radicals detection limits (311.14 nM) (Fig. S9).

Beckman and co-workers first proposed the concept of $ONOO^-$ formation by the non-enzymatic reaction of •NO and $O_2^{\bullet -}$, and expounded the truth that generating of •NO and $O_2^{\bullet -}$ is regulated by NADPH oxidase (NOX) and inducible nitric oxide synthase (iNOS),

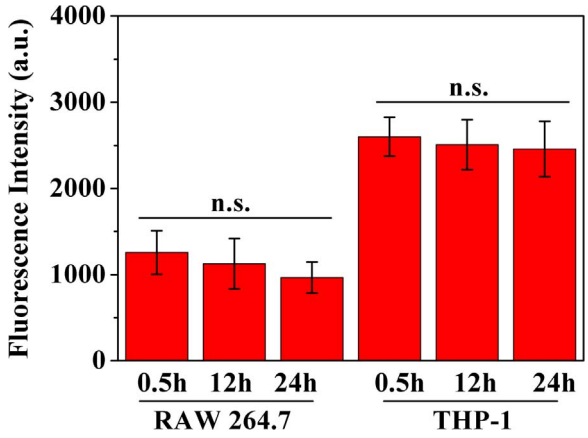

Fig. 2. Fluorescence intensity of F_{482} in murine RAW 264.7 macrophages and human THP-1 cells in absence of a stimulus. Cells were incubated for 0.5 h, 12 h, 24 h before confocal imaging. Fluorescence data were acquired by using red channel λ_{ex}=543 nm, λ_{em}=570–630 nm. Statistical analyses were performed with two-sample *t*-test (n=6 fields of cells). The error bars represent ± S.D.

respectively (Gryglewski, et al., 1986; Beckman et al., 1990; Radi et al., 2001). To validate whether the fluorescence visualization is caused by $ONOO^-$ generation, we conducted an enzyme inhibition test. After pretreatment of the cells with either iNOS inhibitor aminoguanidine (AG, 5 mM) or a NOX inhibitor, apocynin (100 μM) (Peng et al., 2014; Li et al., 2015a, 2015b), the green fluorescence signal of F_{482} was effectively suppressed in the stimulated cells (Fig. 3b1, b2, c1, c2), suggesting that $ONOO^-$ generation was greatly attenuated. These results further confirm that the observed ratiometric fluorescence change of F_{482} in murine RAW 264.7 macrophages is attributed to the $ONOO^-$ generation that is induced from immunostimulation.

The elusive nature of $ONOO^-$, stems from its extremely short half-life (~10 ms) and low steady-state concentration (nM range), making it difficult to quantify in live cells (Szabo et al., 2007). To date, no fluorescence methods are available for the direct quantitation of $ONOO^-$ by a ratiometric approach. According to the calibration curve (F_{green}/F_{red} versus $ONOO^-$ concentration) established in living cells in Fig. S23b, the concentrations of $ONOO^-$ in the murine RAW 264.7 macrophages (Fig. 3b) was estimated to be 655.1 ± 72.5 nM and RSD 11.07%, in agreement with the previously estimated nanomolar steady-state concentration range (Nalwaya and Deen, 2005; Quijano et al., 2005), which demonstrates F_{482} is capable of detecting and quantifying immune-associated $ONOO^-$ in live cells.

To confirm the universality of F_{482} to image and quantify $ONOO^-$ in different phagocyte cell lines, the human THP-1 cell line was adopted to evaluate the capacities of probe. The probe emitted clear red fluorescence after THP-1 cells were incubated with 5 μM F_{482} for 30 min; however, negligible green fluorescence was observed (Fig. S18, S19). The ratio of green/red fluorescence intensities remained unperturbed even after 12 h and 24 h, suggesting F_{482} could even tolerate the oxidative stress in a non-immune-stimulated THP-1 cell line. Furthermore, Fig. 4(a1, a2 and b) shows significant increases in green/red emission ratios localized within the phagosomes compared to other intracellular regions in immune-stimulated cells. These data establish that F_{482} is capable of visualizing immune-stimulated phagocytes. The pretreatment of the cells with either AG (5 mM) or apocynin (100 μM) distinctly reduced green fluorescence (Fig. S20), demonstrating that the observed ratiometric fluorescence changes of F_{482} were attributed to $ONOO^-$ generation.

Our cell imaging experiments using F_{482} provide the direct visualization evidence that immune-associated $ONOO^-$ is indeed generated in human macrophages, and the ratiometric readout provided by this probe allows for detection of highly localized changes in $ONOO^-$ concentrations at phagocytic sites (Fig. 4b1–b3), the Pearson's correlation coefficient of the red and green channel is 0.914, confirmed the detecting reaction toward $ONOO^-$ mostly occurred in the phagosomes. The average basal $ONOO^-$ level in human THP-1 cells (Fig. 4b) was calculated as 666.7 ± 59.9 nM and RSD 8.98%, based on the calibration curve established in Fig. S23b.

To further demonstrate the capacity of F_{482} to quantify $ONOO^-$ in large populations of stimulated macrophages, we conducted a two-color flow cytometry (FCM) analysis in human THP-1 cells. The THP-1 cells were treated with the same procedure mentioned previously. The data dots (Fig. 4c) for different cell groups distributing in different regions indicates the fluorescence intensity of the two channels (FITC-A channel and PE-A channel). The ratio of two mean fluorescence intensities (FITC-A/PE-A) showed an obvious increase from 0.305 to 3.060 after immune-stimulation (Fig. 4d). Interestingly, this 10-fold enhancement is consistent with the data obtained from confocal fluorescence imaging. Thus, we have developed a methodology utilizing the FCM analysis assisted by F_{482} to quantify $ONOO^-$ levels in stimulated THP-1 cells. These results have demonstrated that our method allows for $ONOO^-$ quantification in immune-stimulated phagocytes with high selectivity and sensitivity.

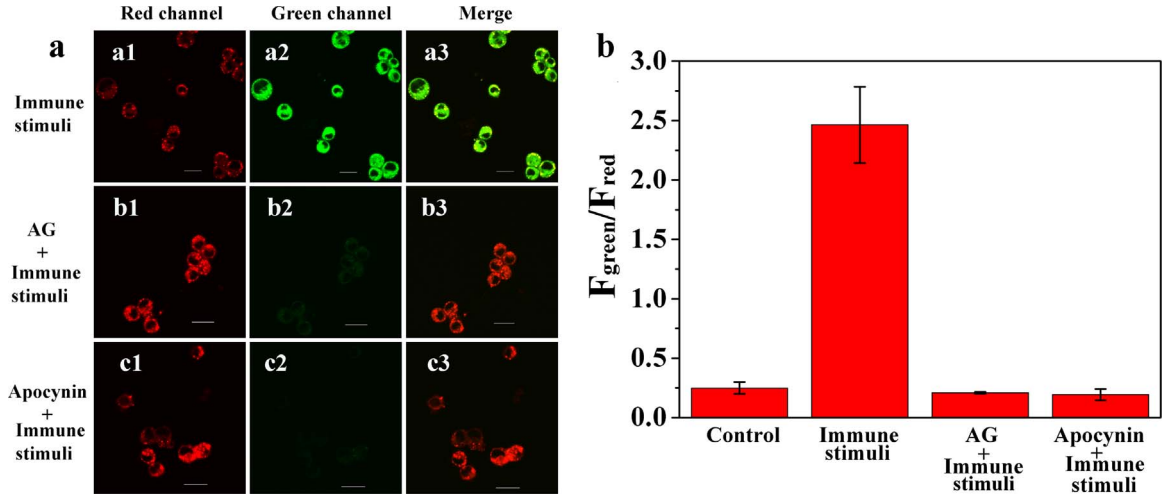

Fig. 3. Confocal fluorescence images of RAW 264.7 macrophages exposed to immune stimulus. RAW 264.7 macrophages were treated with immunostimulation and then loaded with 5 μM F_{482} for 30 min. (a1-a3) LPS (1 μg/ml) for 16 h then PMA (500 nM) for 1 h; (b1-b3) AG (5 mM) for 4 h, LPS (1 μg/ml) 16 h then PMA (500 nM) for 1 h; (c1-c3) Apocynin (100 μM) for 1 h, LPS (1 μg/ml) for 16 h then PMA (500 nM) for 1 h; (b) Relative F_{green}/F_{red} ratios displayed by cells loaded with F_{482}. Scale bar represents 20 μm. The error bars represent ± S.D. (n=12). (For interpretation of the references to color in this figure legend, the reader is referred to the web version of this article.)

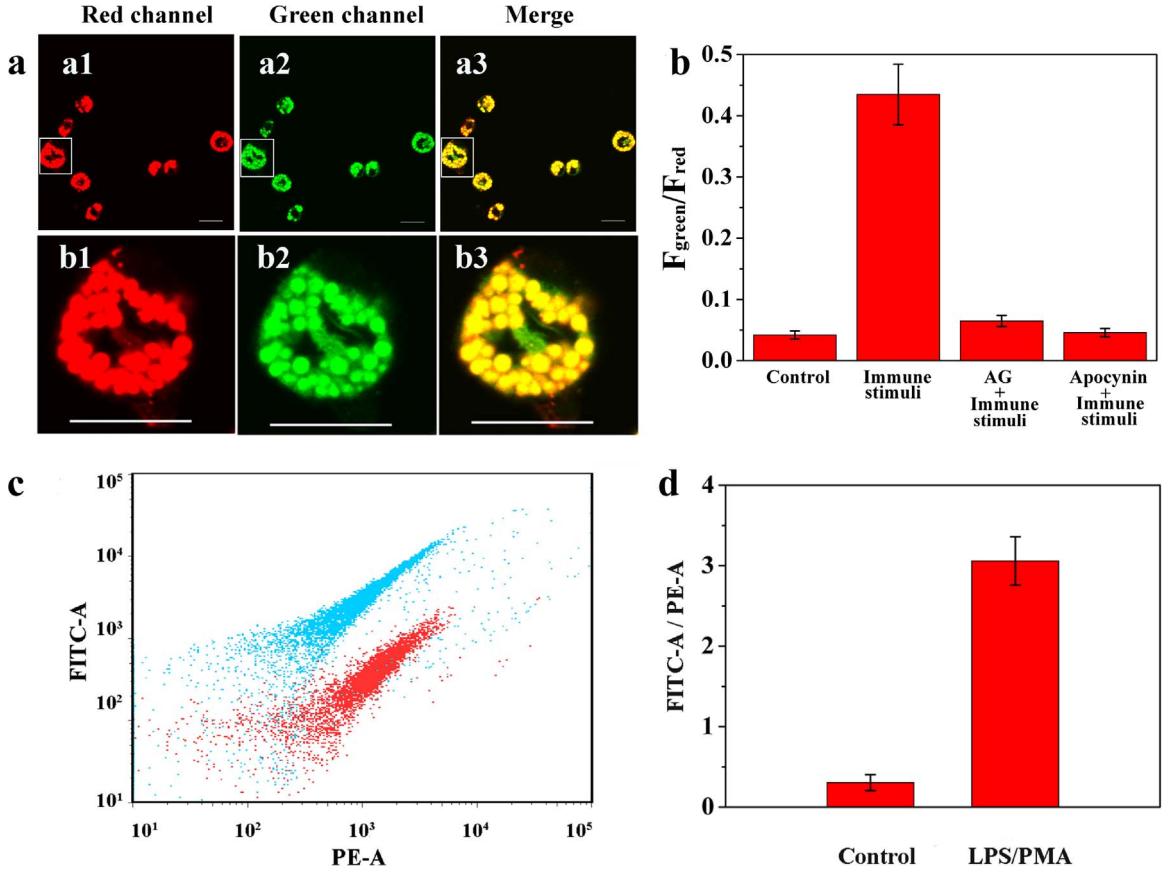

Fig. 4. Confocal fluorescence images of THP-1 cells exposed to immune stimulus. THP-1 cells were treated with immune stimuli and then loaded with 5 μM F_{482} for 30 min. (a1-a3) LPS (1 μg/ml) for 16 h then PMA (500 nM) for 1 h; (b1-b3) Magnified section (indicated by a white box in a1-a3) shows phagosome imaging in immune-stimulated THP-1 cells; (b) Relative F_{green}/F_{red} ratios displayed by cells loaded with F_{482}; (c) Flow cytometry analysis of F_{482}-loaded normal THP-1 cells (red) and stimulated THP-1 cells (blue); (d) Ratiometric mean fluorescence intensity of the green (FITC-A) and red (PE-A) channels displayed by cells stained with F_{482}. Scale bar represents 20 μm. The excitation wavelength was 488 nm. FITC-A channel: 530 ± 30 nm. PE-A channel: 585 ± 42 nm. The error bars represent ± S.D. (n=3). (For interpretation of the references to color in this figure legend, the reader is referred to the web version of this article.)

3.5. In vivo imaging and quantifying $ONOO^-$ in inflammation mouse model

As reported, excessively produced $ONOO^-$ is implicated in the development of numerous inflammatory diseases (Radi, 2013). Thereby, F_{482} was used to evaluate the endogenous $ONOO^-$ levels in a mouse inflammation model. The mice were administered intraperitoneally (i.p.) with lipopolysaccharide (LPS) to induce acute inflammation (Lee et al., 2007). After 4 h, the mice were anaesthetized and their abdominal fur was removed. Then, the mice were injected i.p. with F_{482} and divided into three groups. One group was injected i.p. with saline, the second group was injected with PMA, and the third group was injected with apocynin (4 mM) followed by PMA (Fig. 5a) (Oushiki et al., 2010). Images were acquired using an in vivo imaging system after 30 min. The ratio fluorescence intensity of F_{482} was remarkably increased by approximately 10-fold by PMA stimulation compared to the saline-treated groups and was partially suppressed by apocynin treatment (Fig. 5b).

Another group of mice was injected with LPS into both the right and left rear paws. After 4 h, PMA was injected into right rear paws and saline was injected into the left rear paws (Fig. 5c); then F_{482} was injected through the tail vein. The data acquired from the images show a greater ratio fluorescent intensity compared to the left paws pretreated with saline (Fig. 5d), which indicate that F_{482} is transported and accumulated in inflamed areas and the ratio-metrically imaging of $ONOO^-$ is observed in right paws. Taken together, our experiments demonstrate that F_{482} is capable of imaging inflammation-associated $ONOO^-$ generation in vivo.

4. Conclusions

In summary, we have designed and synthesized two probes (F_{482} and F_{495}) by a Knoevenagel condensation reaction of the BODIPY scaffold with two trans-cinnamaldehyde molecules. F_{482} functions as a specific ratiometric chemosensor that features a stable structure in live cells and a sensitive response toward $ONOO^-$ with a marked red-to-green emission change. The detection limit was as low as 150.54 nM. Significantly, F_{482} can be applied to image basal $ONOO^-$ in immune-stimulated macrophage cells and the $ONOO^-$ generation in phagosomes can be quantified by high-throughput flow cytometry analysis. It is believed that F_{482} provides a promising chemical tool for the study of $ONOO^-$ biology and understanding the molecular mechanism of $ONOO^-$ activity in the inflammatory response process in vitro and in vivo. Current efforts are underway to utilize F_{482} and develop next generation versions to probe the biology of reactive ROS/RNS species, specifically in the context of diseases.

Acknowledgements

This work is supported by the National Basic Research Program of China (2013CB922102) and the National Natural Science Foundation of China (21275072, 21475059 and 21527809). We thank Jun Cai (Nanjing University) for help with in vivo imaging.

Appendix A. Supporting information

Supplementary data associated with this article can be found in the

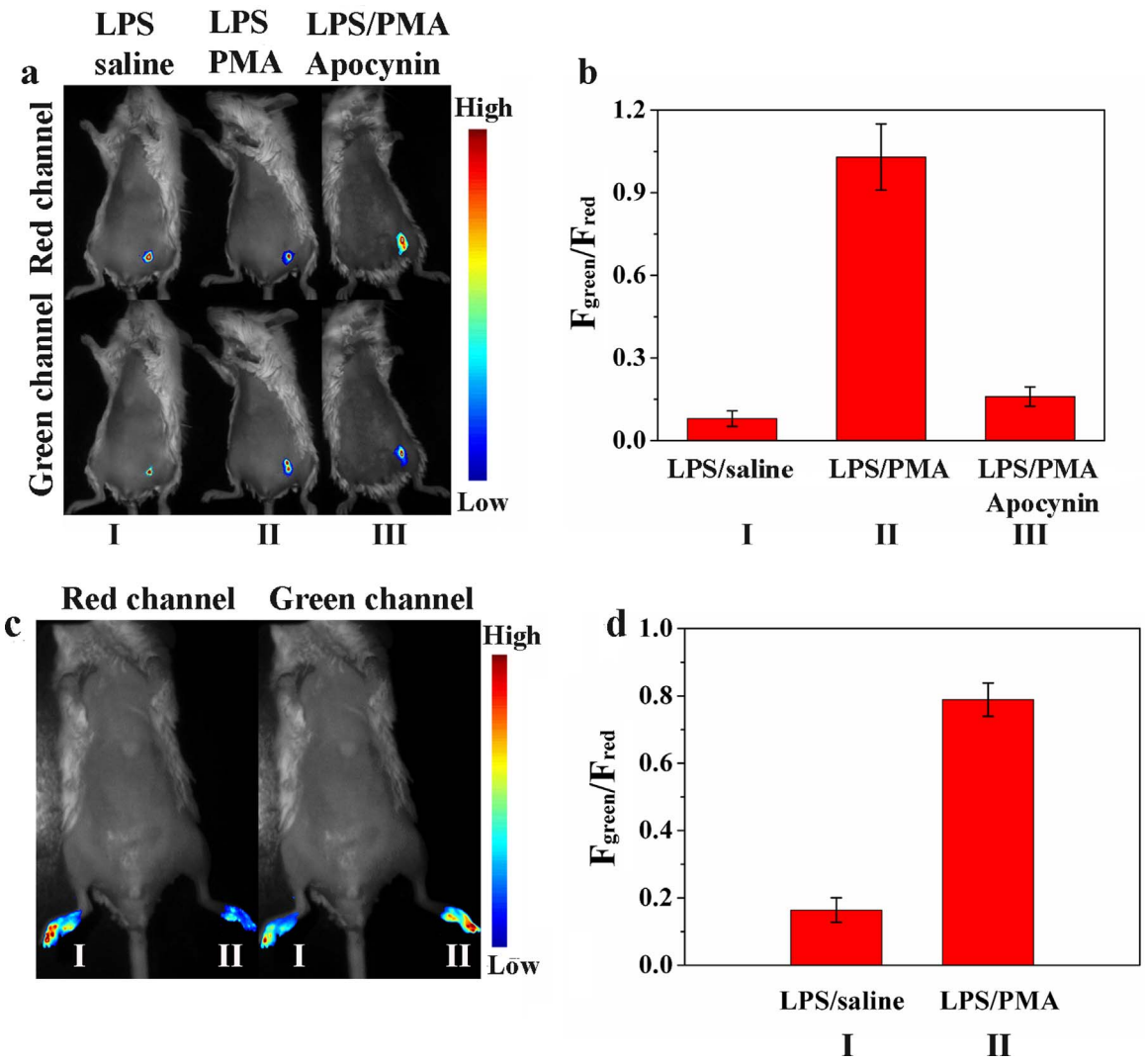

Fig. 5. In vivo imaging of endogenous $ONOO^-$ generation in the peritoneal cavity and inflamed paws of mice via F_{482}. (a) Fluorescence images of LPS-treated mice (I: LPS+saline, II: LPS+PMA, III: LPS+Apocynin+PMA) from the red channel (560–700 nm) and green channel (490–540 nm); (b) Ratiometric fluorescence intensity (F_{green}/F_{red}) of LPS-treated mice 30 min after injecting of F_{482}; (c) The fluorescence images of LPS-treated mice from red channel (560–700 nm) and green channel (490–540 nm). (I) The left paw was injected i.p. with LPS and saline as control, (II) the right paw was injected i.p. with LPS and PMA; (d) Ratiometric fluorescence intensity (F_{green}/F_{red}) of left paws and right paws 30 min after injection with F_{482}. The error bars represent ± S.D. (n=3). (For interpretation of the references to color in this figure legend, the reader is referred to the web version of this article.)

online version at doi:10.1016/j.bios.2016.11.036.

References

Ahmad, R., Rasheed, Z., Ahsan, H., 2009. Immunopharmacol. Immunotoxicol. 31, 388–396.

Alvarez, M.N., Peluffo, G., Piacenza, L., Radi, R., 2011. J. Biol. Chem. 286, 6627–6640.

Barba-Bon, A., Calabuig, L., Costero, A.M., Gil, S., Martinez-Manez, R., Sancenon, F., 2014. RSC Adv. 4, 8962–8965.

Beckman, J.S., Beckman, T.W., Chen, J., Marshall, P.A., Freeman, B.A., 1990. Proc. Natl. Acad. Sci. USA 87, 1620–1624.

Chen, Z.J., Ren, W., Wright, Q.E., Ai, H.W., 2013. J. Am. Chem. Soc. 135, 14940–14943.

De Cremer, G., Roeffaers, M.B.J., Bartholomeeusen, E., Lin, K., Dedecker, P., Pescarmona, P.P., Jacobs, P.A., De Vos, D.E., Hofkens, J., Sels, B.F., 2010. Angew. Chem 122, 920–923, (Angew. Chem. Int. Ed. 49, 908–911).

Denicola, A., Rubbo, H., Rodriguez, D., Radi, R., 1993. Arch. Biochem. Biophys. 304, 279–286.

Drummen, G.P.C., Gadella, B.M., Post, J.A., Brouwers, J.F., 2004. Free Radic. Biol. Med. 36, 1635–1644.

Fang, F.C., 2004. Nat. Rev. Microbiol. 2, 820–832.

Ferdinandy, P.B., 2006. J. Pharmacol. 148, 1–3.

Finkel, T., Holbrook, N.J., 2000. Nature 408, 239–247.

Franco, M.C., Ye, Y., Refakis, C.A., Feldman, J.L., Stokes, A.L., Basso, M., Melero Fernandezde Mera, R.M., Sparrow, N.A., Calingasan, N.Y., Kiaei, M., Rhoads, T.W., Ma, T.C., Grumet, M., Barnes, S., Beal, M.F., Beckman, J.S., Mehl, R., Estevez, A.G., 2013. Proc. Natl. Acad. Sci. USA 110, E1102–E1111.

Gryglewski, R.J., Palmer, R.M., Moncada, S., 1986. Nature 320, 454–456.

Hou, J.T., Yang, J., Li, K., Liao, Y.X., Yu, K.K., Xie, Y.M., Yu, X.Q., 2014. Chem. Commun. 50, 9947–9950.

Hirata, T., Terai, T., Komatsu, T., Hanaoka, k., Nagano, T., 2011. Bioorg. Med. Chem. Lett. 21, 6090–6093.

Lee, D., Khaja, S., Velasquez-Castano, J.C., Dasari, M., Sun, C., Petros, J., Taylor, W.R., Murthy, N., 2007. Nat. Mater. 6, 765–769.

Lee, J.S., Kim, H.K., Feng, S.H., Vendrell, M., Chang, Y.T., 2011. Chem. Commun. 47, 2339–2341.

Lin, K.K., Wu, S.C., Hsu, K.M., Hung, C.H., Liaw, W.F., Wang, Y.M., 2013. Org. Lett. 15, 4242–4245.

Li, X., Tao, R.R., Hong, L.J., Cheng, J., Jiang, Q., Lu, Y.M., Liao, M.H., Ye, W.F., Lu, N.N., Han, F., Hu, Y.Z., Hu, Y.H., 2015a. J. Am. Chem. Soc. 137, 12296–12303.

Li, Z., Geng, Z.R., Zhang, C., Wang, X.B., Wang, Z.L., 2015b. Biosens. Bioelectron. 72, 1–9.

Murray, J., Taylor, W.S., Zhang, B., Ghosh, S.S., Capaldi, A.R., 2003. J. Biol. Chem. 278, 37223–37230.

Nalwaya, N., Deen, W.M., 2005. Chem. Res. Toxicol. 18, 486–493.

Nossaman, B.D., Kadowitz, P.J., 2008. Open Pharmacol. J. 2, 31–53.

Oushiki, D., Kojima, H., Terai, T., Arita, M., Hanaoka, K., Urano, Y., Nagano, T., 2010. J. Am. Chem. Soc. 132, 2795–2801.

Pacher, P., Beckman, J.S., Liaudet, L., 2007. Physiol. Rev. 87, 315–424.

Peng, T., Wong, N.K., Chen, X., Chan, Y.K., Ho, D.H., Sun, Z., Hu, J.J., Shen, J., El-Nezami, H., Yang, D., 2014. J. Am. Chem. Soc. 136, 11728–11734.

Quijano, C., Romero, N., Radi, R., 2005. Free Radic. Biol. Med. 39, 728–741.

Rurack, K., Kollmannsberger, M., Daub, J., 2001. Angew. Chem 113, 396–398, (Angew. Chem. Int. Ed. 40, 385-387).

Radi, R., 2013. J. Biol. Chem. 288, 26464–26472.

Radi, R., Peluffo, G., Alvarez, M.A., Naviliat, M., Ocayota, A., 2001. Free Radic. Biol. Med.

30, 463–488.
Ronson, R.S., Nakamura, M., Vinten-Johansen, J., 1999. Cardiovasc. Res 44, 47–59.
Sun, M., Yu, H., Zhu, H., Ma, F., Zhang, S., Huang, D., Wang, S., 2014. Anal. Chem. 86, 671–677.
Szabo, C., Ischiropoulos, H., Radi, R., 2007. Nat. Rev. Drug Discov. 6, 662–680.
Ueno, T., Urano, Y., Kojima, H., Nagano, T., 2006. J. Am. Chem. Soc. 128, 10640–10641.
Uppu, R.M., Nossaman, B.D., Greco, A.J., Fokin, A., Murthy, S.N., Fonseca, V.A., Kadowitz, P., 2007. J. Clin. Exp. Pharmacol. Physiol. 34, 933–937.
Wang, D.P., Shiraishi, Y., Hirai, T., 2011. Chem. Commun. 47, 2673–2675.
Yang, D., Wang, H.L., Sun, Z.N., Chung, N.W., Shen, J.G., 2006. J. Am. Chem. Soc. 128, 6004–6005.
Zhang, Q., Zhu, Z., Zheng, Y., Cheng, J., Zhang, N., Long, Y.T., Zheng, J., Qian, X., Yang, Y., 2012. J. Am. Chem. Soc. 134, 18479–18482.
Zhu, L., Gunn, C., Beckman, J.S., 1992. Arch. Biochem. Biophys. 298, 452–457.
Zielonka, J.S., kora, A., Joseph, J., Kalyanaraman, B., 2010. J. Biol. Chem. 285, 14210–14216.